

Near real-time detection of atmospheric water vapour using the SADC GPS network

A.Z.A. Combrink^{a,b*}, W.L. Combrinck^a and H. Moraal^b

The Global Positioning System (GPS) has been used for more than a decade for the accurate determination of position on the Earth's surface, as well as for navigation. The system consists of approximately thirty satellites, managed by the US Department of Defense, orbiting at an altitude of 20 200 km, as well as thousands of stationary ground-based and mobile receivers. It has become apparent from numerous studies that the delay of GPS signals in the atmosphere can also be used to study the atmosphere, particularly to determine the precipitable water vapour (PWV) content of the troposphere, and the total electron content of the ionosphere. This paper gives an overview of the mechanisms that contribute to the delay of radio signals between satellites and receivers. The discussion then turns to techniques developed at the Hartebeesthoek Radio Astronomy Observatory's Space Geodesy Programme to estimate tropospheric delays (from which PWV is calculated) in near real-time, using the SADC (Southern African Development Community) Network of dual-frequency GPS receivers. Opportunities for future work are also discussed.

Introduction and background

Radio astronomers, space geodesists and meteorologists all have an interest in the amount of water vapour in the atmosphere, for various reasons. To the radio astronomer observing electromagnetic waves at the centimetre wavelength level, atmospheric water vapour is a nuisance, causing absorption and emission at these wavelengths. Atmospheric water vapour also causes satellites, used in space geodetic techniques, to appear farther than they really are, as a result of the refraction of electromagnetic waves and the assumption of a constant vacuum propagation velocity used in the determination of their distances. Accurate measurements of water vapour enable radio astronomers and space geodesists to correct their observations by including it in tropospheric models.

Meteorologists bring atmospheric water vapour a little closer to the man in the street. The atmosphere's water vapour content is an extremely important parameter in numerical weather prediction. The high cost of radiosondes (weather balloons) — currently the only source of water vapour data — has forced the South African Weather Service (SAWS) to reduce the number of launches to a maximum of two per day, at only seven selected sites inside South Africa (D. Esterhuyse, 2004, pers. comm.).

The Global Positioning System (GPS) offers a solution. (A thorough description of the Global Positioning System, its specifications and an exact description of its working are given by Hoffmann-Wellenhof *et al.*¹) If the position of a ground-based GPS station and the orbit of a GPS satellite are known, one can calculate how long it should take for a radio signal to travel between the two, assuming that the signal travels at the speed of

light in vacuum. Refraction caused by the ionosphere and the troposphere results in a delay, from which the tropospheric precipitable water vapour (PWV) content and the ionospheric total electron content (TEC) can be calculated.

Two networks of dual-frequency GPS receivers, which can be used for geodetic purposes, exist in southern Africa. Figure 1 shows the distribution of these stations. Ten stations, set up by Hartebeesthoek Radio Astronomy Observatory's (HartRAO's) Space Geodesy Programme in collaboration with JPL (NASA's Jet Propulsion Laboratory), NRCan (Natural Resources Canada), NOAA (National Oceanic and Atmospheric Administration, US Department of Commerce) and GFZ Potsdam (GeoForschungZentrum), form the SADC (Southern African Development Community) IGS (International GPS Service) network. Trignet, consisting of approximately thirty stations, is the network established and maintained by the Chief Directorate: Surveys and Mapping (CDSM).

The research described in this paper aims to determine whether it will be possible to determine PWV from observational GPS data, using the existing SADC GPS network.

The positions of these GPS receiver antennas have been accurately established (to the millimetre level). Assuming that one also knows the satellite orbits, one can calculate from Einstein's second postulate how long it should take for radio signals to travel the distance between a specific satellite and receiver. The fundamental observable in GPS is the propagation time of a signal transmitted from the GPS satellite. However, as the radio signals travel through the atmosphere, they undergo refraction and delay relative to the propagation time in vacuum, owing to the phase velocity being different from that in vacuum. As a result of this refraction, they neither travel in a straight line nor at the speed of light in vacuum (c). However, the increased path length due to the refraction is negligible compared to the apparent increase in path length resulting from the decrease in the phase velocity. Therefore, we will consider the transport of electromagnetic waves in matter and indicate how the delay experienced by a radio wave in the troposphere can be used to estimate the atmospheric water vapour content.

The transport and delay of electromagnetic waves in the atmosphere

For our purposes, we divide the atmosphere into two parts:

- the neutral part, termed the troposphere. It actually includes the troposphere, stratosphere, ozonosphere and the lower part of the mesosphere, extending over altitudes of 0–70 km; and
- the partially charged part, which is called the ionosphere. This is made up of the upper mesosphere and the thermosphere, and forms at an altitude above 70 km.

We now derive the refractivity and resultant delay of a signal in each of these parts of the atmosphere.

Ionospheric delay

The ionosphere is the upper, partially ionized part of the atmosphere, which is responsible for the absorption and reflection

^aSpace Geodesy Programme, Hartebeesthoek Radio Astronomy Observatory, P.O. Box 443, Krugersdorp 1740, South Africa.

^bUnit for Space Physics, School of Physics, North-West University, Private Bag X6001, Potchefstroom 2520, South Africa.

*Author for correspondence. E-mail: attie@hartrao.ac.za

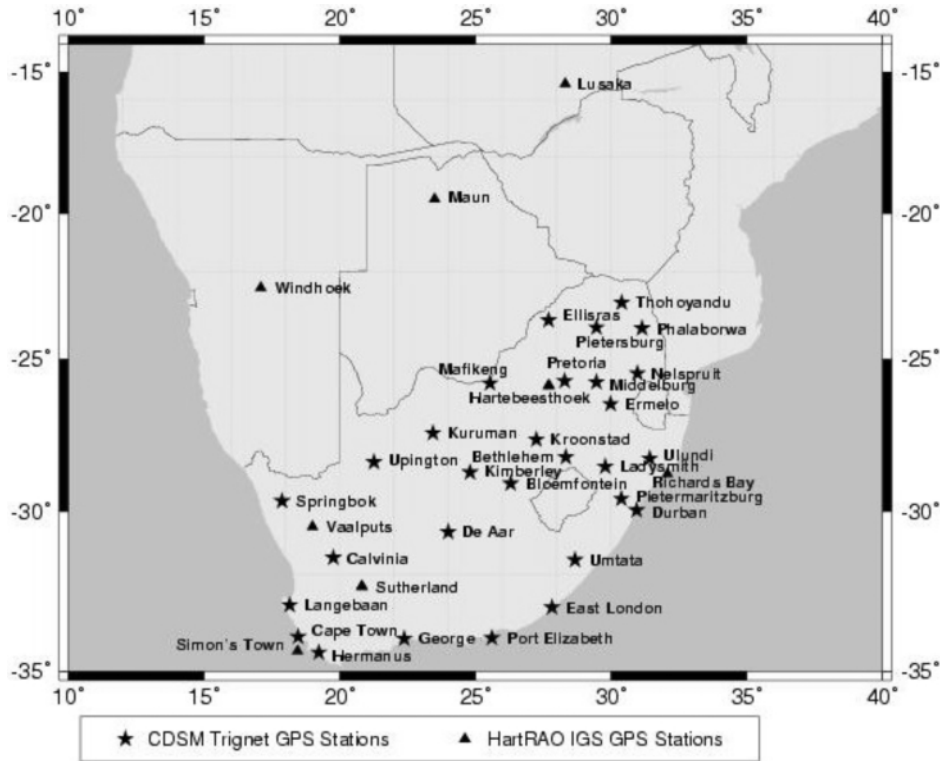


Fig. 1. The two existing GPS networks in southern Africa are HartRAO's SADC IGS network (▲) and the Chief Directorate: Surveys and Mapping's Trignet (★).²

of radio waves at low frequencies (generally below 25 MHz). Molecules and atoms in the upper atmosphere are ionized by absorbing radiation energy from the Sun. Free electrons and ions in the ionosphere are also attributed to ion exchange between the ionosphere and the plasmasphere above it. Free electrons and ions in the ionosphere continuously recombine, so that only a fraction of the molecules and atoms are ionized at any given time.

The ionosphere is characterized by its content of free electrons and ions. The F₂ layer of the ionosphere has the highest density of charged particles,³ with values up to 3 × 10¹² m⁻³.

The total electron content (TEC)⁴ is defined as the number of electrons in a column of unit area cross section along the trans-ionospheric ray path, written as

$$E_T = \int_0^{h_0} N \cdot dh, \tag{1}$$

where *N* is the spatial density of electrons, *h* is the coordinate of propagation of the wave, and *h*₀ corresponds to the effective top of the ionosphere.

TEC is highly variable and depends on several factors, such as local time, geographical location (latitude in particular), season and solar activity. TEC can have values between 1 TECU (or TEC unit, defined as 10¹⁶ m⁻²) and 10³ TECU.³

Because the ionosphere is partially charged, one expects that the propagation of electromagnetic waves will differ drastically from the tropospheric case. We can therefore derive the refractivity of the ionosphere, following Chen⁵ and Choudhuri.⁶

For electromagnetic waves traversing a non-magnetized plasma, the dispersion relation

$$\omega^2 = \omega_p^2 + c^2 k^2 \tag{2}$$

holds, where the plasma frequency ω_p is defined by $\omega_p^2 \equiv n_0 e^2 / \epsilon_0 m$, with *n*₀ the number density of electrons, *-e* and *m* are respectively the charge and mass of an electron, ϵ_0 the permittivity of vacuum, *c* the speed of light in vacuum, and *k* the

wave number.

One can also write this as $ck = \omega \sqrt{1 + (\omega_p / \omega)^2}$. Recalling that phase and group velocities are defined as $v_{phase} \equiv \omega / k$ and $v_{group} \equiv \frac{\partial \omega}{\partial k} = \frac{\partial}{\partial k} \left(\frac{ck}{n(k)} \right) = \frac{c}{n(\omega) + \omega (dn/d\omega)}$, respectively, with *n*(ω) the conventional index of refraction, and that phase and group indices of refraction are defined as $n_p \equiv c/v_{phase}$ and $n_g \equiv c/v_{group}$, respectively, two indices of refraction can be defined as

$$n = \sqrt{1 \mp (\omega_p / \omega)^2}, \tag{3}$$

where the negative sign applies to phase velocities and the positive sign to group velocities.

GPS satellites emit signals at two frequencies, namely, 1.57542 GHz (L₁) and 1.22760 GHz (L₂). For these frequencies, $\omega_p / \omega \ll 1$ and by means of the binomial expansion $\sqrt{1 \pm \epsilon} \approx 1 \pm \frac{1}{2} \epsilon$, (3) becomes

$$n \approx 1 \mp 1/2 (\omega_p / \omega)^2. \tag{4}$$

Defining the refractivity of the ionosphere as $N_e \equiv n - 1$, we obtain

$$N_e \approx \mp 1/2 (\omega_p / \omega)^2 = \mp 40.3 \text{ Hz}^2 \text{ m}^3 \text{ f}^{-2} n_0. \tag{5}$$

In the ionosphere, *n*₀ is typically of the order of 10¹² m⁻³, so that the refractivity of an L₁ signal in the ionosphere is typically $N_e \approx \mp 1.6 \times 10^{-5}$.

For vertical incidence of radio waves, the correction to the path distance of the waves, i.e. the experienced delay through the ionosphere, is defined as

$$\Delta L_e \equiv \int_0^{\infty} N_e(z) dz, \tag{6}$$

with *z* the coordinate of propagation.

Thus, from (1) and (5), the vertical path correction for the

ionosphere is given by

$$\Delta L_e = \mp 40.3 \text{ Hz}^2 \text{ m}^3 \text{ f}^{-2} \int_0^\infty n_0(z) dz = \mp 40.3 \text{ Hz}^2 \text{ m}^3 \text{ f}^{-2} E_T \quad (7)$$

with E_T the so-called 'total electron content'⁶ in m^{-2} , as defined in (1). A typical value of the TEC is $50 \text{ TECU} = 5 \times 10^{17} \text{ m}^{-2}$, so that the experienced ionospheric delay of an L_1 signal is $\approx \mp 8 \text{ m}$.

The refractivity and delay of the L_2 signal is a factor $(1.57542/1.22760)^2 \approx 1.65$ larger than for the L_1 signal. It is therefore easy to correct for the ionospheric delay and these ionospheric corrections are being done very accurately by GPS processing software, to the submillimetre level in path length.

Tropospheric delay

Griffiths⁷ makes a model of dispersion that takes place on an atomic scale in a dielectric substance, such as the neutral part of the Earth's atmosphere (troposphere), to derive the Cauchy equation. The derivation is only an approximation of the quantum mechanical model, but yields satisfactory results nevertheless. This model describes the electron as a damped harmonic oscillator, driven by an electromagnetic wave of frequency ω . The derived Cauchy equation, in terms of wavelength $\lambda = 2\pi c/\omega$, is

$$n = 1 + N_n (1 + B/\lambda^2), \quad (8)$$

with n the index of refraction of the troposphere, N_n the refractivity and B the dispersion coefficient. B was found to be $1.7 \times 10^{-14} \text{ m}^2$ for the troposphere.⁸

The typical radio wavelengths we consider are of the order of 0.2 m (L-band), so that $B/\lambda^2 \ll 1$, and consequently $N_n \approx n - 1$, so that the propagation of radio waves in the troposphere is non-dispersive.

The refractivity of the troposphere is typically $N_n \approx 4 \times 10^{-6}$, so that from (6) it follows that the tropospheric delay is $\Delta L_n \approx 2 \text{ m}$, or about 25% of the delay of the L_2 signal in the ionosphere.

We now determine the delay of an incoming radio wave in terms of the apparent length added to the signal's path. Take $\Delta L(\theta)$ to be the geometric delay (or additional apparent path length) of the radio wave, with θ the elevation angle of the direction from which the wave arrives, as shown in Fig. 2. Let S be the true path along which the radio wave propagates and G the shortest geometric path along which the signal would travel if $n = 1$. Then

$$\Delta L(\theta) = \int_S n ds - G = \int_S (n-1) ds + (S-G). \quad (9)$$

The first term of (9) refers to the delay of a signal due to its reduced speed in the troposphere, while the second term refers to the geometric delay due to the bending of the signal, which can be neglected for elevation angles greater than 15° .⁹ We can therefore approximate $S = \int_S ds \approx G$, so that $\Delta L(\theta) = \int_S (n-1) ds = \int_S N ds$.

The tropospheric zenith delay $\Delta L^z \equiv \Delta L(90^\circ)$, conventionally abbreviated as ZTD, is one of the quantities estimated by the GAMIT GPS processing software. GAMIT, which is discussed later, is well-documented and a critical evaluation of it is beyond the scope of this paper. The rms error in the ZTD estimated by GAMIT is strongly dependent on the data quantity and quality, but usually below one centimetre.

Delay due to water vapour

We now calculate N , and the consequent delay experienced by a radio wave in the troposphere, as a function of the precipitable water vapour content (PWV) of the troposphere, and pressure and temperature measured at ground level. This enables one to

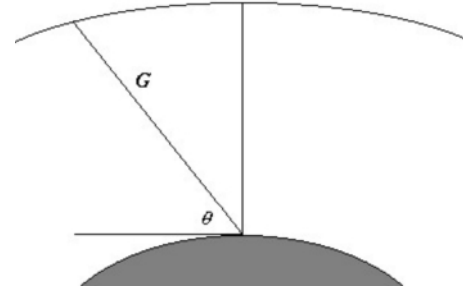


Fig. 2. Radio signals from a GPS satellite arrive at a ground-based receiver, from a direction with an associated elevation angle θ above the horizon, travelling along an electrical (true) path; for elevation angles greater than 15° the electrical path can be approximated by the shortest geometric path G .

estimate PWV from the pressure, the temperature and the delay of a radio wave measured at ground level.

For the troposphere, consisting of, say, q gases, the delay depends on the density ρ_i of each gas. Following Gradinarsky,⁹ we write

$$N = \sum_{i=1}^q \rho_i (A_i + B_i/T), \quad (10)$$

as first derived by Debye.¹⁰ T is the temperature in kelvin (K) and A_i and B_i are constants for each gas. In the case of monatomic and diatomic gases, and CO_2 , which account for the largest part of the atmosphere, $B_i = 0$. However, this is not the case for H_2O , because of its permanent dipole moment. In his classical work, Debye¹⁰ gives a quantitative explanation for the temperature dependence of water's coefficient of refraction. This means that, because the water molecules are permanent electric dipoles, one has to treat atmospheric water vapour and the 'dry' gases in the atmosphere separately.

The equation of state for the atmosphere's i th component, with Z_i the dimensionless compressibility, is $p_i V = Z_i n_i R_i T$, where the gas constant of the i th component is defined as $R_i = R/M_i$, with $R = 8.31 \text{ J K}^{-1} \text{ mol}^{-1}$, the universal gas constant, and M_i the molar mass; all other symbols have their usual meaning. Using $\rho_i = n_i V$, it is clear that $\rho_i = p_i/(Z_i R_i T)$, so that (10) becomes

$$N = \sum_d A_d p_d / (Z_d R_d T) + A_w p_w / (Z_w R_w T) + B_w p_w / (Z_w R_w T^2),$$

where distinction has been made between water vapour (w) and the dry gases (d). This can also be expressed as

$$N = k_1 p_d T^{-1} Z_d^{-1} + k_2 p_w T^{-1} Z_w^{-1} + k_3 p_w T^{-2} Z_w^{-1}, \quad (11)$$

with k_i constants under the assumption of a uniform distribution of atmospheric constituents, and p_d and p_w the partial pressure of the dry and wet components, respectively.¹¹ The first term of (11) can be written in terms of the total density, $\rho = \rho_d + \rho_w$. Defining $k'_2 = k_2 - k_1 M_w M_d^{-1}$, with M_w and M_d the molar masses of the water vapour and dry air respectively, (11) becomes

$$N = k_1 R_d \rho + k'_2 p_w T^{-1} Z_w^{-1} + k_3 p_w T^{-2} Z_w^{-1}. \quad (12)$$

It is assumed that the condition of hydrostatic equilibrium,

$$dp/dz = -\rho(z)g(z), \quad (13)$$

is satisfied, with $g(z)$ the gravitational acceleration and $\rho(z)$ the mass density at a height z , and p the total pressure. The first term of (12), which is the hydrostatic component of N , can now be written as $N_h = k_1 R_d \rho$. From (13) the hydrostatic delay is then expressed as:

$$\Delta L_n = \int_S N_h ds = \int_z k_1 R_d \rho(z) dz = k_1 R_d p_0 g_m^{-1}, \quad (14)$$

with p_0 the total pressure at the base and g_m the mean gravita-

tional acceleration of the vertical column. According to the model proposed by Saastamoinen,¹² $g_m = 9.8062(1 - 2.66 \times 10^{-3} \times \cos 2\lambda - 2.8 \times 10^{-7}H) \text{ m s}^{-2}$, with λ the latitude and H the height (in m) above the ellipsoid.

Davis *et al.*¹³ give the values of the following constants: $k_1 = 77.604 \pm 0.014 \text{ K mb}^{-1}$ and $M_d = 28.9644 \pm 0.0014 \text{ g mol}^{-1}$. Substituting this into (14), the hydrostatic delay is $\Delta L_h(\text{m}) = [(2.2768 \pm 0.0005) \times 10^{-3}] \frac{p_0(\text{mb})}{f(\lambda, H)}$, with $f(\lambda, H) = 1 - 2.66 \times 10^{-3} \cos(2\lambda) - 2.8 \times 10^{-7} H(\text{m})$.

The second and third terms of Equation (12) are the 'wet' components of N , and can be written as

$$N_w = [k'_2 p_w T^{-1} + k_3 p_w T^{-2}] Z_w^{-1} \tag{15}$$

The mean temperature of the vertical column of water vapour is defined as

$$T_m = \int \frac{p_w}{T} dz / \int \frac{p_w}{T^2} dz \tag{16}$$

From (15) and (16) the delay due to tropospheric water vapour is then expressed as

$$\Delta L_w = [k'_2 + k_3 T_m^{-1}] \int_s p_w T^{-1} Z_w^{-1} ds \tag{17}$$

The equation of state for water vapour can be written in the form $p_w T^{-1} Z_w^{-1} = n R V^{-1}$, where all the symbols have their usual meanings. The right-hand side can further be written in terms of the specific gas constant R_w and molar mass M_w of water, so that $p_w T^{-1} Z_w^{-1} = n R_w M_w V^{-1} = D \rho_w R_w$, with ρ_w the density of water (10^3 kg m^{-3}) and D the relative density of the precipitable water vapour in the troposphere. Thus, the total precipitable water vapour content of the troposphere, $PWV = \int_s D ds$, is given by

$$PWV = (\rho_w R_w)^{-1} \int_s p_w T^{-1} Z_w^{-1} ds = k(T_{\text{surface}}) \Delta L_w \tag{18}$$

with $k(T_{\text{surface}}) = [\rho_w R_w (k'_2 + k_3 T_m^{-1})]$ and the mean temperature approximated as $T_m = 70.2 \text{ K} + 0.72 T_{\text{surface}}$, following Bevis *et al.*¹⁴ Further, $k'_2 = 22.1 \text{ K hPa}^{-1}$, $k_3 = 3.739 \times 10^5 \text{ K}^2 \text{ hPa}^{-1}$ and $R_w = 4.614 \times 10^2 \text{ J K}^{-1} \text{ kg}^{-1}$, according to Borbás.¹⁵

Therefore, the ZTD is the sum of the hydrostatic and wet delay components, i.e. $\Delta L^z = \Delta L_h + \Delta L_w$, and PWV can be calculated from ZTD if pressure and temperature measurements are available. The hydrostatic delay (14) is typically in the range 1.7–2.1 m; it does not vary much at a specific site and depends mainly on the site's altitude. Although hydrostatic delay is the main contributor to the total delay, the wet delay is the main contributor to variation in the total delay, with values ranging between zero and 40 cm, depending on local meteorological conditions.

Very few, if any, GPS observations are made at zenith. The tropospheric delay at an arbitrary elevation angle, θ is expressed as a function of hydrostatic and wet delays, ΔL_i , and mapping functions, $m_i(\theta)$, respectively:

$$\Delta L(\theta) = \Delta L_h m_h(\theta) + \Delta L_w m_w(\theta) \tag{19}$$

Thus, through the use of mapping functions, one can map the zenith delay to a delay that a signal would experience at an arbitrary elevation angle.

If the atmosphere in the vicinity of a GPS station is uniform, a simple sine function can be used to map the zenith delay ΔL^z to the delay for an arbitrary elevation angle θ :

$$\Delta L(\theta) = \Delta L^z / \sin \theta \tag{20}$$

This mapping function is sufficient for elevation angles $\theta > 20^\circ$;

for lower elevation angles, more complex functions must be used to account for the curvature of the Earth.⁹

The Niell Mapping Function (NMF), proposed by Niell,¹⁶ is most commonly used in space geodesy, because it is presently believed to be the most accurate at elevation angles from 90° down to below 10° , and it does not require any meteorological observations. It was also employed in the processing of GPS observational data for this project. The NMF is of the form

$$m(\theta) = \left(1 + \frac{a}{1 + \frac{b}{1+c}} \right) / \left(\sin \theta + \frac{a}{\sin \theta + \frac{b}{\sin \theta + c}} \right) \tag{21}$$

with a , b and c different parameters for the hydrostatic and wet mapping functions, which also vary with latitude. Extensive research on the comparison of different mapping functions was done by Rocken *et al.*,¹⁷ but an extensive discussion is beyond the scope of this paper.

The acquisition and processing of GPS data

HartRAO serves as a regional data centre for the International GPS Service (IGS). Currently, about 30 IGS stations' observational data, from January 1998 to the present, are stored at HartRAO and can be obtained from <ftp://geoid.hartrao.ac.za/rinex/>.¹⁸ The data are stored in RINEX (Receiver INdependent EXchange) format, containing 24-hour data sets.

Hourly RINEX files can be obtained from the SOPAC (Scripps Orbit and Permanent Array Center) ftp site at <ftp://garner.ucsd.edu/> for near real-time applications, and are usually published within one hour of observations. The TEQC (Translate/Edit/Quality Check) software package, which can be downloaded from <http://www.unavco.ucar.edu/software/teqc/teqc.html>, was used to concatenate an arbitrary number of hourly RINEX files into a single file. This strategy was applied to both the observational files and the RINEX navigational files, required by the GAMIT processing software described below.

The predicted and precise orbits of the satellites can both be obtained from the SOPAC ftp site. The predicted orbits, which are used for the near real-time processing, have an accuracy of $\sim 25 \text{ cm}$, while the precise orbits, which are used for precise geodetic measurements, have an accuracy of less than 5 cm , but are only available after ~ 13 days. These accuracies are relevant for the along-orbit as well as the across-orbit coordinates of the satellites.

Only data from the following IGS stations were available for the near real-time determination of zenith tropospheric delays over southern Africa (i.e. the 1-hour RINEX files of these stations were made available hourly): HRAO (HartRAO, Hartebeesthoek), SUTH (SAAO, Sutherland), SUTM (GFZ Potsdam, Sutherland), SIMO (Simon's Town), RBAY (Richards Bay), MALI (Malindi, Kenya), DAV1 (Davis, Antarctica), MAW1 (Mawson, Antarctica), LPGA (La Plata, Argentina) and MAS1 (Maspolomas, Canary Islands).

To estimate the tropospheric delay during post-processing, observational data (24-hour RINEX files) from another 13 IGS stations could be obtained from the HartRAO ftp archive.

The Department of Land Affairs' Chief Directorate: Surveys and Mapping (CDSM) has set up a network of approximately 30 permanent GPS receivers in South Africa, called Trignet. The observational data from seven of these stations were also made available for day 154 of 2003: BFTN (Bloemfontein), DRBN (Durban), MFKG (Mafikeng), NSPT (Nelspruit), PELB (Port Elizabeth), SBOK (Springbok) and TRGE (Mowbray).

The GAMIT GPS processing software used for this project was

developed at the Massachusetts Institute of Technology by R. King, T. Herring and several co-workers. The software is freely distributed for use in scientific research, and a licence for the software can be obtained from the authors at <http://www-gpsg.mit.edu/~simon/gtgk/index.html>.

GAMIT was initially designed to process GPS data in 24-hour sets for high-precision geodetic measurements, using precise satellite ephemerides, published weekly by the IGS. Some software scripts were written and some GAMIT input tables were changed to adapt the software for our specific purpose, namely to estimate tropospheric parameters in near real-time, with arbitrary data spans, and utilizing predicted satellite ephemerides.

GAMIT incorporates a weighted least squares algorithm to estimate the positions of stations, orbital and earth rotation parameters, and atmospheric delays, by fitting it to doubly-differenced phase observations, which are derived from the carrier beat phase observations using difference-operator algorithms. These algorithms are described by King.¹⁹

Graphical results were generated with the Generic Mapping Tools (GMT programs), which can also be obtained freely from <http://gmt.soest.hawaii.edu/>. The results are in PostScript (*.ps) format.

Optionally, the ImageMagick programs 'convert' and 'animate' (available from <http://www.imagemagick.org/>) can be used to convert the PostScript files to GIF images (*.gif) and generate an animation of a series of images.

All the programming for this project was done in CShell, running the scripts under the LINUX Debian (Woody version, kernel version 2.2) operating system on a Pentium II-266-MHz personal computer. Processing time is strongly dependent on the data quantity and processor speed; it is usually in the order of tens of minutes.

Results of PWV determination

To be included in operational numerical weather predictions, PWV estimates have to be available in near real-time. Figure 3 presents comparisons of zenith tropospheric delay as calculated during post-processing by IGS, and in near real-time by HartRAO. The HartRAO product uses predicted satellite orbits in its hourly estimation of ZTD, whereas the IGS ZTD product is generated only after the precise satellite orbits have been published by the IGS, approximately two weeks after the GPS observations have been made. The IGS product also combines several estimations of ZTD from different global processing centres, using different processing software, and 24-hour data sets are processed to obtain ZTD estimates; the HartRAO product includes only 6-hour data sets to minimize processing time. One can see that the HartRAO near real-time product generally agrees, within the uncertainties, with the IGS post-processed product; a regression analysis yielded a correlation coefficient $r^2 = 0.91$. However, the uncertainties associated with the IGS estimates are approximately four times smaller than those associated with the near real-time estimates; this can be attributed to the approximately four times more accurate satellite ephemerides used to obtain the post-processed product. As connectivity in southern Africa improves, ensuring the availability of all stations' data every hour, and as the satellite orbit predictions become more accu-

ZTD Comparison: IGS Post-Processed vs HartRAO Near Real-Time

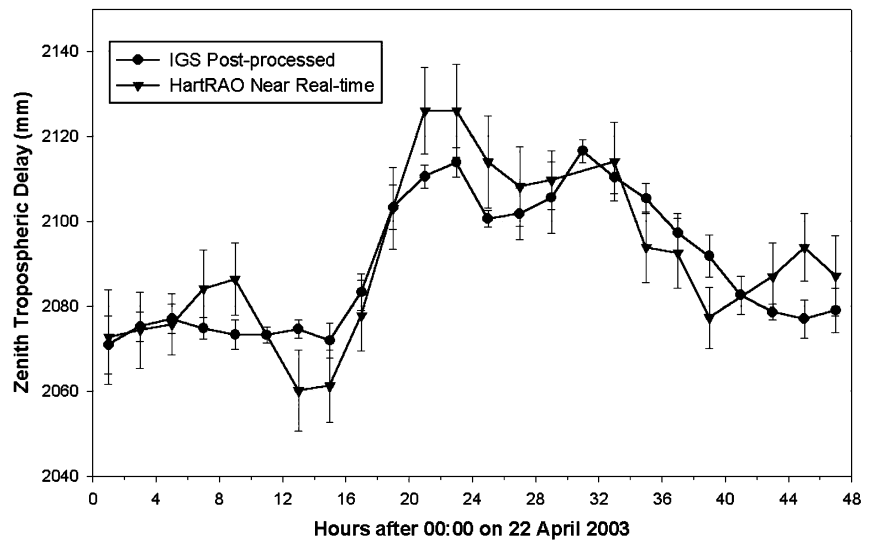


Fig. 3. A comparison of the zenith tropospheric delay (ZTD) as calculated by HartRAO and IGS for the IGS GPS station HRAO. The HartRAO estimates generally agree with the IGS post-processed estimates.

rate, the near real-time estimates of ZTD should correlate even better with the post-processed product.

To estimate the ZTD at a station, GPS observational data are usually processed in a regional network. Figure 4 shows a regional map of ZTD estimated for South Africa and the surrounding oceans by using the data from the hourly IGS stations and Trignet.

Unfortunately, all GPS receivers are not collocated with weather stations or meteorological units. As shown in Equations (17) and (21), measurements of the temperature and pressure are required to determine the precipitable water vapour from the estimated ZTD. Assuming uniform temperatures over the subcontinent and hydrostatic equilibrium in the troposphere, one is able to make rough estimates of the distribution of water vapour over South Africa, as shown in Fig. 5.

Both qualitative and quantitative attempts have been made to verify the results obtained. Figure 6 shows a satellite image of southern Africa at 12:00 UT on day 154 of 2003. This can be compared qualitatively with the maps in Fig. 5, showing clouds associated with a front of moist air over the northeastern part of South Africa that correlate well with the regions of high PWV.

Estimates of PWV were also compared quantitatively with data from radiosondes. The South African Weather Service launches one radiosonde daily from De Aar in the Northern Cape. The CDSM GPS station, collocated with the SAWS weather station at De Aar, was used to estimate zenith delays, while pressure and temperature measurements from the radiosonde were used to obtain the GPS-derived PWV. The radiosonde-derived PWV is compared with the GPS-derived PWV in Fig. 7.

A strong correlation exists between these two data sets; comparison yielded a correlation coefficient r^2 of 0.89 and a regression coefficient b of 1.13. This demonstrates the usefulness of the technique.

Conclusion and future work

Software was developed to estimate tropospheric delays from GPS observational data in near real-time, and have it available for any potential users. From these delays one can derive the atmospheric water vapour content. The results obtained compare well with zenith delay estimates from IGS and water vapour

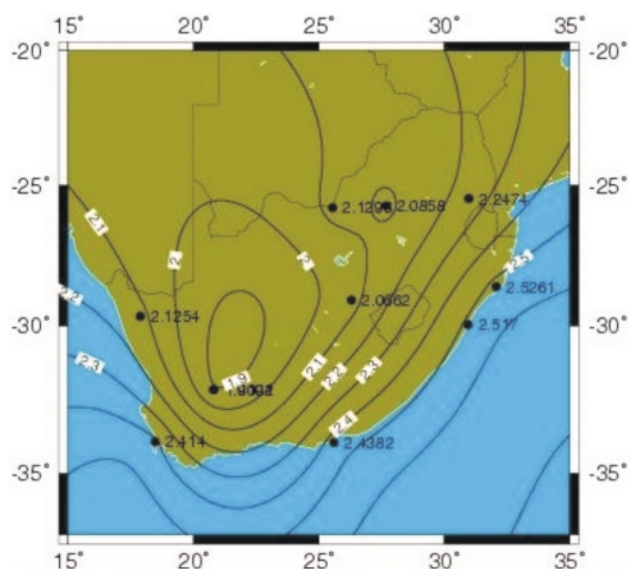


Fig. 4. An isoline map of the zenith tropospheric delay over South Africa for 12:00 UT on day 154 of 2003. The unit of the isolines and point values is metres.

measurements from SAWS.

The use of water vapour measurements to improve tropospheric models used for satellite laser ranging (SLR) is currently being investigated by the ILRS Refractivity Study Group. Combrink²⁰ has shown that the accuracy of SLR estimates of site velocities and positions can be improved by up to 70% and 6.2%, respectively, by including GPS-derived water vapour estimates in tropospheric models.

The inclusion of GPS-derived PWV in operational numerical weather prediction models is also being investigated locally. In the near future, further verification of PWV estimates will be done at GPS sites collocated with SAWS stations from where radiosondes are launched.

Centimetre wavelength radio astronomy, to be performed at HartRAO in the near future, requires estimates of water vapour to correct measured intensities; the technique and theory presented by Combrink²⁰ to determine the tropospheric water vapour content can readily be implemented by radio astronomers.

Apart from future work to be done in the fields of SLR, numerical weather prediction and radio astronomy, total electron content mapping will also be investigated as a potential product for the scientific community, comparing TEC results obtained with those using other techniques, such as digital ionosondes and riometers.

Increasing the number of stations in the southern African GPS network is high on the priority list of HartRAO's Space Geodesy Programme. Given the remoteness of many IGS GPS stations, the lack of connectivity reduces the number of stations that can be used to produce near real-time tropospheric estimates. Connectivity between GPS stations and the database at HartRAO will also be investigated, so that the spatial resolution of results can be improved.

HartRAO is in the process of setting up a computer cluster as a powerful real-time processing tool. This will enable the inclusion of more stations' data for near real-time processing to improve both the spatial and temporal resolution of results.

Finally, this paper demonstrates that the network of dual-frequency receivers in southern Africa can, apart from its use in geodetic research and surveying, be used as a remote sensing tool for the troposphere and ionosphere and that some exciting research in this field lies ahead.

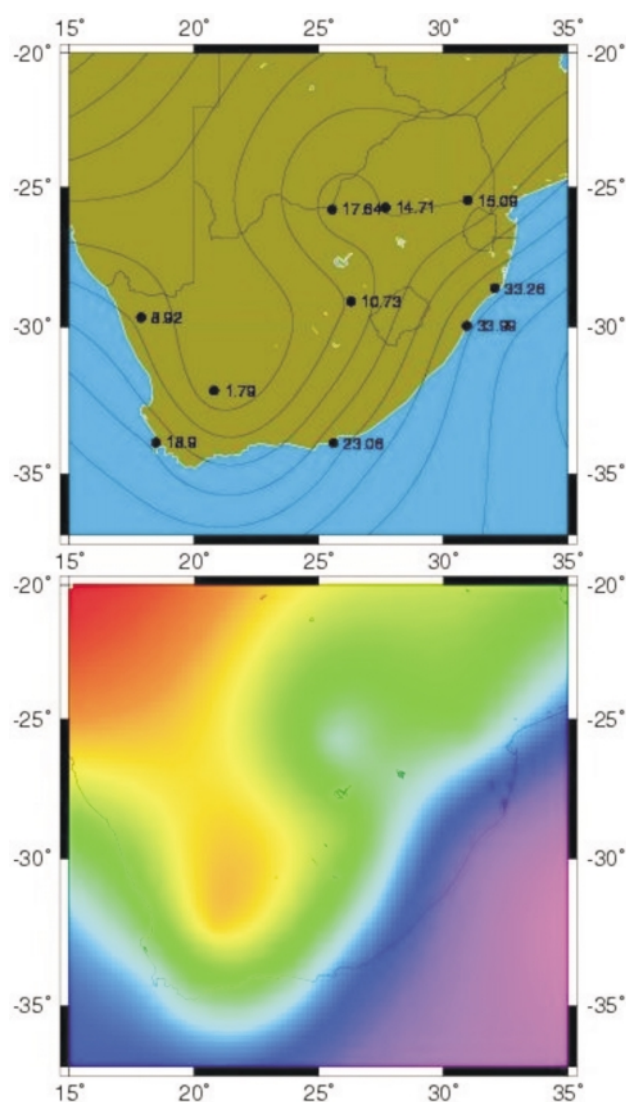


Fig. 5. The distribution of precipitable water vapour (PWV) over South Africa at 12:00 UT on day 154 of 2003. The isoline map (top) shows the absolute PWV (in mm), whereas the colour-enhanced isoline map (bottom) shows the relative PWV, with cooler colours representing more, and warmer colours less, water vapour. These maps were generated from the estimated ZTD under the assumptions of hydrostatic equilibrium and uniform temperatures over the subcontinent.



Fig. 6. A satellite image of the southern African subcontinent at 12:00 UT on day 154 of 2003 (obtained from <http://www.eumetsat.de/>; copyright © 2003 EUMETSAT).

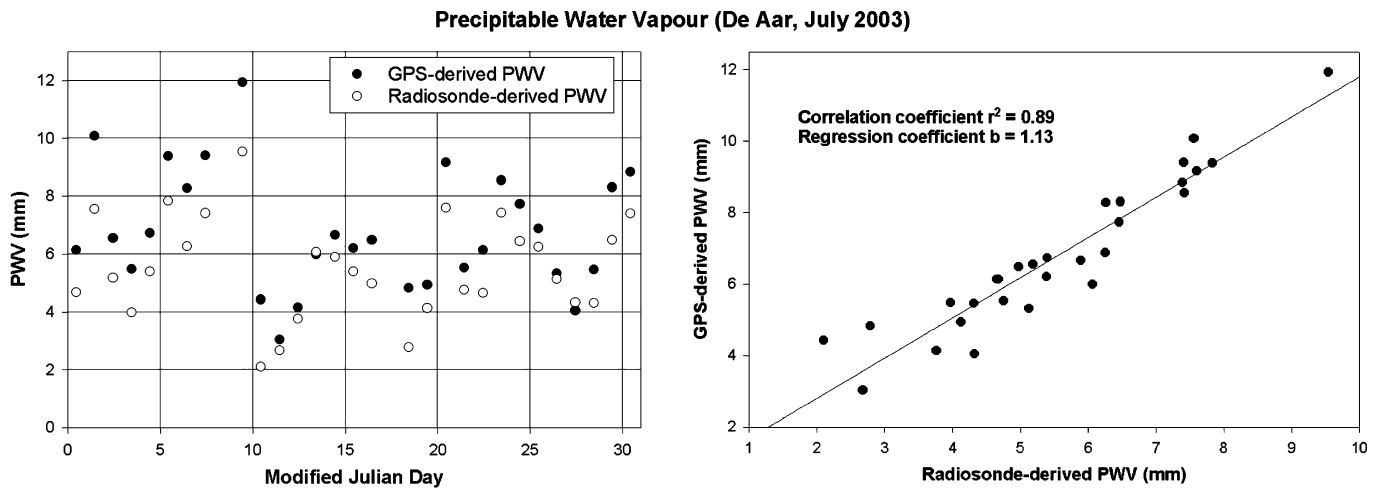


Fig. 7. Comparisons of precipitable water vapour (PWV) for July 2003, obtained from GPS observations and radiosonde launches at De Aar.

We thank Richard Wonnacott of CDSM for supplying some of the GPS data used for this paper. We further thank Danie Esterhuysen of SAWS for supplying the De Aar upper-air data.

Received 19 April. Accepted 28 May 2004.

1. Hoffmann-Wellenhof B., Lichtenegger H. and Collins J. (1993). *GPS — Theory and Practice*, 2nd edn. Springer Verlag, New York.
2. Cilliers P.J., Gouws D., Opperman B., Wonnacott R.T. and Combrinck L. (2003). The South African network of dual-frequency global positioning system satellite receiver base stations: a national asset with many applications and research opportunities. *S. Afr. J. Sci.* **99**, 51–55.
3. Ros E., Marciade J.M., Guirado J.C., Sardón E. and Shapiro I.I. (2000). A GPS-based method to model the plasma effects in VLBI observations. *Astron. Astrophys.* **356**, 357–362.
4. Lynn K.J.W. and Gubbay J.S. (1975). *The Effect of the Earth's Atmosphere on Baseline Determinations by Very Long Baseline Interferometry*, p. 8. Australian Defence Scientific Service, Salisbury.
5. Chen F.F. (1984). In *Introduction to Plasma Physics and Controlled Fusion*, 2nd edn, pp. 114–116. Plenum Press, New York.
6. Choudhuri A.R. (1998). In *The Physics of Fluids and Plasmas*, pp. 239–243. Cambridge University Press, Cambridge.
7. Griffiths D.J. (1999). In *Introduction to Electrodynamics*, 3rd edn, pp. 398–404. Prentice Hall, Upper Saddle River.
8. Riepl S. and Schlüter W. (2000). *Normal Point Algorithm for Reduction of Two Colour SLR Observations*. Online: <http://www.wetzell.ifag.de/publ/2cnp1/nizza.html>.
9. Gradinarsky L. (2000). *Remote sensing of small-scale structures of atmospheric water vapor*, pp. 12–15. Licentiate of Engineering thesis, Chalmers University of Technology, Göteborg.
10. Debye P. (1929). In *Polar Molecules*, pp. 30–35. Dover Publications, New York.
11. Emardson T.R. (1998). *Studies of atmospheric water vapour using the Global Positioning System*, p. 5. Ph.D. thesis, Chalmers University of Technology, Göteborg.
12. Saastamoinen J. (1972). Atmospheric correction for the troposphere and stratosphere in radio ranging of satellites. *The Use of Artificial Satellites for Geodesy* **15**, 247–251.
13. Davis J.L., Herring T.A., Shapiro I.I., Rogers A.E.E. and Elgered G. (1985). Geodesy by radio interferometry: effects of atmospheric modelling errors on the estimates of the baseline length. *Radio Sci.* **20**(6), 1593–1609.
14. Bevis M., Businger S., Herring T.A., Rocken C., Anthes R.A. and Ware R.H. (1992). GPS meteorology: remote sensing of atmospheric water vapour using the Global Positioning System. *J. Geophys. Res.* **97**(D14), 15787–15801.
15. Borbás É. (1997). Determination of precipitable water for a fixed site using the Global Positioning System technique. *Q. J. Hung. Met. Serv.* **101**(4), 261–273.
16. Niell A.E. (1996). Global mapping functions for the atmosphere delay at radio wavelengths. *J. Geophys. Res.* **101**, 3227–3246.
17. Rocken C., Sokolovskiy S., Hunt D. and Johnson J.M. (2001). Improved mapping of tropospheric delays. *J. Atmos. Ocean. Tech.* **18**, 1205–1213.
18. Combrinck W.L. (1999). *The HartRAO Space Geodesy Programme*. Online: http://www.hartao.ac.za/geodesy/geodesy_index.html.
19. King R. (2002). *Documentation for the GAMIT GPS Analysis Software*. Online: <http://chandler.mit.edu/~simon/gtgk/GAMIT.pdf>.
20. Combrinck A.Z.A. (2003). *Detection of Atmospheric Water Vapour using the Global Positioning System*, pp. 46–47. M.Sc. dissertation, Potchefstroom University for CHE, Potchefstroom.